

Article

Development of an In-Situ Simulation Device for Testing Deep Pressure-Preserving Coring Tools under High-Temperature and Ultrahigh-Pressure Conditions

Wei Huang ¹, Heping Xie ^{1,2,3}, Jianan Li ², Yang Yang ², Cong Li ^{2,3}, Zhiqiang He ^{2,3}, Yihang Li ² and Zetian Zhang ^{2,*}

¹ School of Mechanical Engineering, Sichuan University, Chengdu 610065, China

² College of Water Resource & Hydropower, Sichuan University, Chengdu 610065, China

³ Guangdong Provincial Key Laboratory of Deep Earth Sciences, Geothermal Energy Exploitation and Utilization, Institute of Deep Earth Sciences and Green Energy, College of Civil and Transportation Engineering, Shenzhen University, Shenzhen 518060, China

* Correspondence: zhangzetian@scu.edu.cn

Abstract: With the increasing mining depth of deep mineral resources, the underground temperature and pressure also increase, which requires more advanced mining equipment. Therefore, to adapt to the special application scenario of the research and development of pressure-preserving coring tools under the extreme environmental conditions of deep strata, in this study, an in-situ simulation device under high-temperature and ultrahigh-pressure conditions is developed. The principles and methods of applying temperature and pressure to the device are expounded. Furthermore, the two main modules of the device are analyzed and studied experimentally. On the one hand, a segmented simulated coring test cabin is constructed, and pressure testing of the test cabin is carried out. The results show that the test cabin with inner diameters of 150 mm and 500 mm runs stably under the working condition of a pressure up to 190 MPa (considering the influence of temperature of 150 °C), and the cabin remains in the stage of elastic deformation. There is no leakage of pressure or fluid in the whole test process. On the other hand, the performance of the driving module is tested. The results show that the driving module can provide a stable rotation speed of up to 150 r/min when the sealing pressure is 140 MPa. Therefore, the device can be applied to carry out simulated coring test and is suitable for the research and development of pressure-preserving coring tools in deep extreme environments, which may promote the development of deep mining engineering.

Keywords: coring simulation device; high-temperature; ultrahigh-pressure; pressure-preserving coring tools



Citation: Huang, W.; Xie, H.; Li, J.; Yang, Y.; Li, C.; He, Z.; Li, Y.; Zhang, Z. Development of an In-Situ Simulation Device for Testing Deep Pressure-Preserving Coring Tools under High-Temperature and Ultrahigh-Pressure Conditions. *Appl. Sci.* **2023**, *13*, 3889. <https://doi.org/10.3390/app13063889>

Academic Editor: Abílio Manuel Pinho de Jesus

Received: 13 February 2023

Revised: 15 March 2023

Accepted: 17 March 2023

Published: 18 March 2023



Copyright: © 2023 by the authors. Licensee MDPI, Basel, Switzerland. This article is an open access article distributed under the terms and conditions of the Creative Commons Attribution (CC BY) license (<https://creativecommons.org/licenses/by/4.0/>).

1. Introduction

With the continuous exploitation of global resources, the number of deep and ultradeep holes is increasing, and the pressure and temperature of the occurrence environment at the bottom of holes are also increasing [1–4]. Because the physical and chemical properties of rocks in deep in-situ environments are quite different from those under normal temperature and pressure [5], it is very important to obtain in-situ rock samples and study their related properties to realize effective evaluation of deep resources [6–8]. At the same time, a high-temperature and high-pressure environment will impact the engineering of deep drilling projects. When the resource mining depth exceeds 1000 m, a series of mining accidents will occur because existing rock theory cannot provide theoretical support for the development of deep mining technology [9,10]. Therefore, it is urgent to evaluate rock theory in a deep in-situ state to promote the development of deep mining technology.

During the exploration of deep rock, it is important to retrieve cores with their in-situ pressure conditions to more accurately simulate the occurrence environment (temperature

and pressure) of deep rock samples [11–14]. According to cores obtained in recent decades, deep cores undergo cracking and destruction as they are brought to the surface, which changes their original composition and characteristics. This phenomenon is caused by the lack of means necessary to maintain the pressure environment of the core as it is raised from the bottom of the hole to the surface and exposed on the ground; this changes the environment of the core, results in the release of internal stress, and alters the composition [15–21]. Therefore, it is of great significance to study the physical and mechanical properties of bottom-hole rock with deep cores for which the in-situ pressure is preserved. To achieve this goal, it is necessary to simulate the deep temperature and pressure environment first, because this provides an experimental environment for the development of coring tools compatible with high pressures and solves the problems of high-risk and high-cost for on-site coring tests.

The simulation of a high-temperature and ultrahigh-pressure environment can be used to verify the performance of a pressure-preserving coring tools in deep environments. At present, research institutions have carried out considerable research on downhole simulation test devices and have made some progress [22–26]. Ekei et al. used an indoor micro-drill to conduct drilling tests on rock samples subjected to lithostatic pressure, pore pressure, and drilling fluid column pressure at the same time, and studied the effects of fluid properties and pressure on the drilling speed of rock samples [27]. Schlumberger Cambridge Research Center in the UK has established a drilling simulation test facility that can be used to study the mechanical properties of drill bits and rocks [28]. This facility can provide a pressure environment with a maximum overburden pressure of 17.9 MPa, a lithostatic pressure of 103.5 MPa, and a pore pressure and drilling fluid column pressure of 69 MPa, and achieve the highest simulation temperature of 200 °C. Terra Tek, Inc. [29,30] has developed a full-scale simulation drilling test device to simulate downhole pressure, which is as follows: overburden pressure of 207 MPa, lithostatic pressure of 138 MPa, pore pressure of 27.6 MPa, and liquid column pressure of 103 MPa. A series of important conclusions in the field of drilling have been obtained by using standard tricone bits to drill rock samples. The simulation test device manufactured by the Comprehensive Research Institute of Resources and Environment Technology of the Ministry of Industry and Technology of Japan can complete the simulation of temperature and pressure environment of the stratum with a depth of 6000 m at the bottom of the well [31], in which the compressive stress of overlying strata can be simulated to be 135 MPa, pore pressure and liquid column pressure to be 50 MPa, and lithostatic pressure to be 100 MPa. The test unit can simulate the drilling of rock samples with a diameter of 215.9 mm or less. The full-size drilling simulation test device developed by the Belm Branch of the Drilling Technology Research Institute of the former Soviet Union in Russia used a rock sample with a diameter of 260 mm and a length of 1500 mm in the simulation drilling test [31,32]. The device can simulate the temperature and pressure environment of rock occurrence at the bottom of the well at 20,000 m, mainly used for the study of rock physical characteristics. The Institute of Exploration Technology of the Ministry of Geology and Mineral Resources developed the M150 simulation wellbore with a maximum simulated pressure of 2.45 MPa and a simulated temperature of 150 °C [33]. The China National Petroleum Corporation (CNPC) has established a drilling tool test system at the Daguang Oilfield [34], which is mainly used to test the reliability of drilling tools. Its maximum simulated temperature is 180 °C, and its maximum pressure is 60 MPa. Wei Linshan et al. [35] designed a set of high-temperature and high-pressure simulation test systems for instrument development and used them to test the safety and reliability of sensitive instrumental components in high-temperature and high-pressure environments. Pang Dongxiao et al. [36] developed a high-temperature and high-pressure experimental device for downhole tools, and it performed loading and torsion tests on tools inside the wellbore. The high-temperature and high-pressure downhole tool experimental device developed by Xu Dingjiang et al. [37] was used to conduct performance evaluation experiments on various downhole tools, such as packers and throttles. Zhang Weihong et al. [38] developed a simulation test device for

downhole tools in vertical holes, and it simulates the working conditions under formation temperature and pressure. The device can simulate test functions for downhole tools with different specifications, including heating, loading, pressurization, and circulation of oil casings. Though these studies were designed by research groups in different fields for different purposes and requirements, all of them have important value. However, most studies have only simulated the downhole pressure environment, and few have simulated the temperature. Meanwhile, these devices are mainly used to study rock properties and bit performance. Very few are dedicated to the development of coring tools, and even fewer are dedicated to the research of pressure-preserving coring tools. Therefore, the development of an in-situ high-temperature and ultrahigh-pressure device for deep pressure-preserving coring tools is described in this paper. The goal is to build a test system capable of simulating a maximum pressure of 140 MPa and a maximum temperature of 150 °C to carry out experimental research on pressure-preserving coring tools in deep extreme environments. The research and development of such a device is of great significance to the mining engineering of deep resources.

2. Principle and Structure of the In-Situ Simulation Device for Deep Coring Tools

2.1. The Structure and Design Principle of the Device

A high-temperature and ultrahigh-pressure simulation test for deep coring tools must have a strictly controlled working environment. The simulation test device is a comprehensive test system that comprises two parts: a high-temperature and ultrahigh-pressure simulation test cabin and a driving module for simulating coring tests, as shown in Figure 1. High-temperature and ultrahigh-pressure simulation test cabins can be used to simulate the in-situ occurrence environment of underground rock. The driving module for simulating coring tests provides a power source for the coring tools and allows it to realize rotation and downward vertical action and ultrahigh-pressure dynamic sealing. The key design specifications of the in-situ simulation device were as follows:

- (1) Maximum working pressure of the test cabin: 140 MPa;
- (2) Maximum operating temperature of the test cabin: 150 °C;
- (3) Maximum working pressure of the driving module: 140 MPa;
- (4) Maximum rotation speed of the driving module: 150 r/min;
- (5) Inner diameter of the rock cabin: 500 mm;
- (6) Inner diameter of the drill pipe cabin: 150 mm.

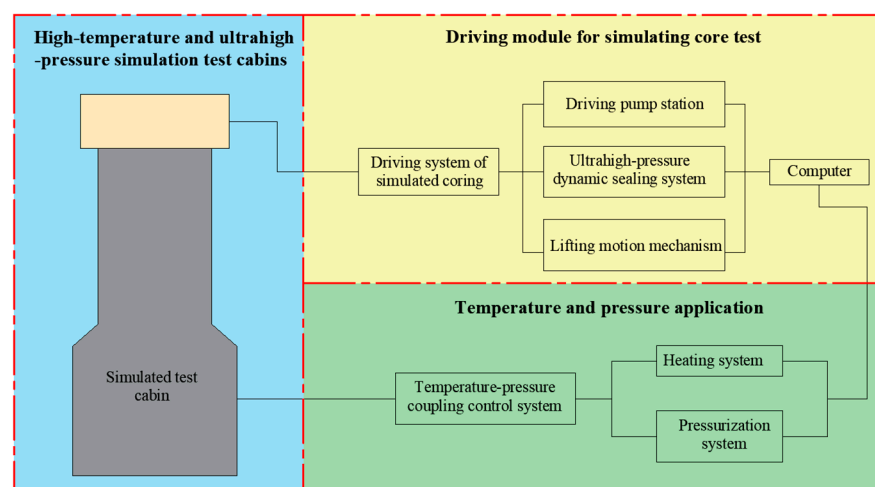


Figure 1. Schematic diagram of the in-situ simulation device.

In addition to meeting the requirements for the temperature, pressure, and size parameters described above, the simulation device should follow these design principles [22–24]: (1) safety and reliability; (2) economy (the costs of design, materials, processing, and

manufacturing should be reduced as much as possible, as long as the components meet the use requirements); (3) easy maintenance; and (4) simple application (the design and manufacture of the whole test chamber system should adopt existing structural forms and processing technology as much as possible, with simple application as the goal).

2.2. Principle of Temperature and Pressure Application

(1) Analysis of the stress state of underground rock

In the deep earth environment, rocks are mainly subjected to multidirectional compressive stress. In the actual drilling and coring process, the pressure on bottom-hole rock in a high-temperature environment is due to four compressive stresses: overburden pressure, lithostatic pressure, pore pressure, and drilling fluid column pressure. The stress state of rock is illustrated in Figure 2 [31].

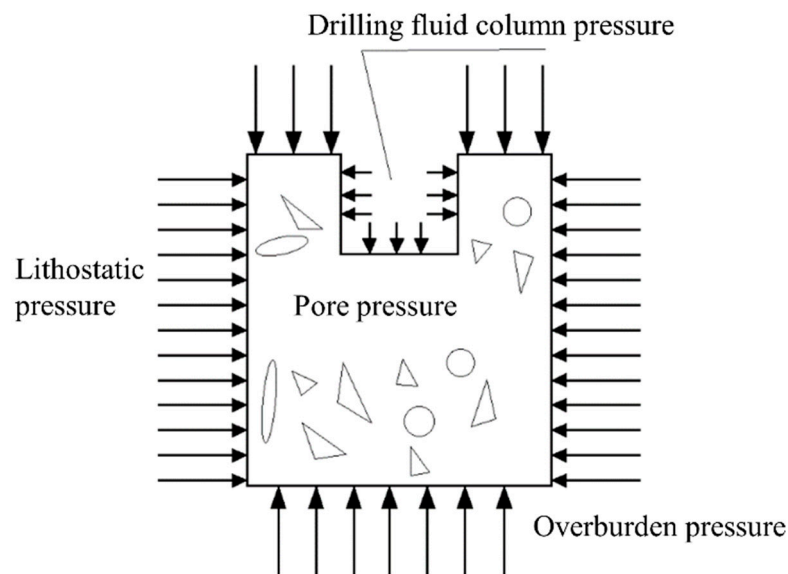


Figure 2. Stress state of rock at the bottom of the hole.

The overburden pressure is caused by the vertical downward pressure exerted by rocks in the upper strata. Lithostatic pressure is the lateral pressure exerted by rocks in the surrounding strata. Due to the presence of pores in the rock, the fluid in the pores provides pore pressure. Fluid column pressure is caused by the unavoidable use of drilling fluid during drilling, which exerts pressure on the rock.

(2) Temperature and pressure application method

The principle for applying temperature and pressure is shown in Figure 3. To apply overburden pressure on rock samples, a pressure oil cylinder is added in the lower part of the rock cabin, the pressurized hydraulic oil enters the lower end face of the piston, and the piston applies the overburden pressure on the upper face of the rock sample. The overburden pressure can be adjusted by adjusting the oil pressure on the lower end of the piston, and finally, an overburden pressure of 140 MPa is applied to the rock sample.

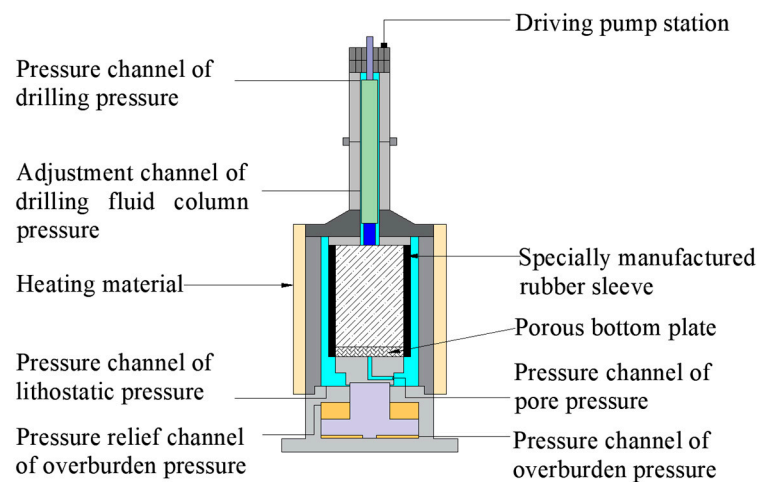


Figure 3. Schematic diagram of temperature-pressure application.

A special rubber sleeve is used to wrap the rock sample, and the outer cylindrical surface of the rock sample and the inner wall of the rock cabin form a closed pressurized space. Then, the high-pressure pump forces high-temperature and high-pressure water into the space. The rock sample rubber sleeve applies pressure perpendicular to the sample surface, which provides lithostatic pressure on the rock sample. To apply pore pressure, the high-temperature and high-pressure water added by the high-pressure pump is injected into a hole through a pore in the middle of the upper cover of the piston, flows to the porous bottom plate, and then penetrates upward from the bottom of the rock sample. The drilling fluid column pressure is added by regulating the back pressure with a throttle valve installed in a high-pressure line in the return hole of the first drill pipe cabin.

The outer layer of the rock sample chamber is wrapped with a layer of heating material to apply heat to the rock sample. Although the pressurized oil in the bottom oil cylinder is at normal temperature, the lithostatic pressure, pore pressure, and drilling fluid column pressure are established with a high-temperature and high-pressure water with a temperature of 150 °C, which also applies heat to the whole test cabin. Additionally, the use of clear water as a heating and pressurizing medium reflects the actual drilling process.

3. Analysis and Design of Key Components

3.1. High-Temperature and Ultrahigh-Pressure Simulation Test Cabin

With the requirements of high-pressure resistance and a large pressure vessel, the material and structure of the pressure vessel must be strictly controlled. In practical engineering, vessels with design pressures between 10 and 100 MPa are generally called high-pressure vessels, and those with design pressures exceeding 100 MPa are called ultrahigh-pressure vessels. The maximum working pressure of the coring simulation test chamber proposed in this paper is 140 MPa, so it belongs to the category of ultrahigh-pressure vessels.

3.1.1. Overall Structure of the Simulation Test Cabin

The high-temperature and ultrahigh-pressure simulation test chamber is used to create the downhole environment and accommodate large rock samples, and it must also meet operating space requirements for the coring tester. The overall structure is shown in Figure 4. The chamber consists of two main parts. The first part is the rock sample chamber, which contains a $\text{Ø}480 \times 1500$ mm rock sample to be drilled. Based on the application space needed for control of the four pressures and the temperature acting on the rock sample, the inner diameter of the rock sample chamber is set at 500 mm, and the length is 2400 mm. The second part is the drill pipe cabin located in the upper part of the core cabin. Based on the operational size requirements of the core, the drill pipe cabin is divided into two sections. The length of the first drill pipe cabin is 2 m, the length of the second drill pipe

cabin is 3 m, and both are 150 mm in diameter. During simulation tests, the coring device is put into the drill pipe cabin to simulate the coring of rock samples in the rock cabin. In addition, an intermediate transition cabin and the bottom oil cylinder are included.

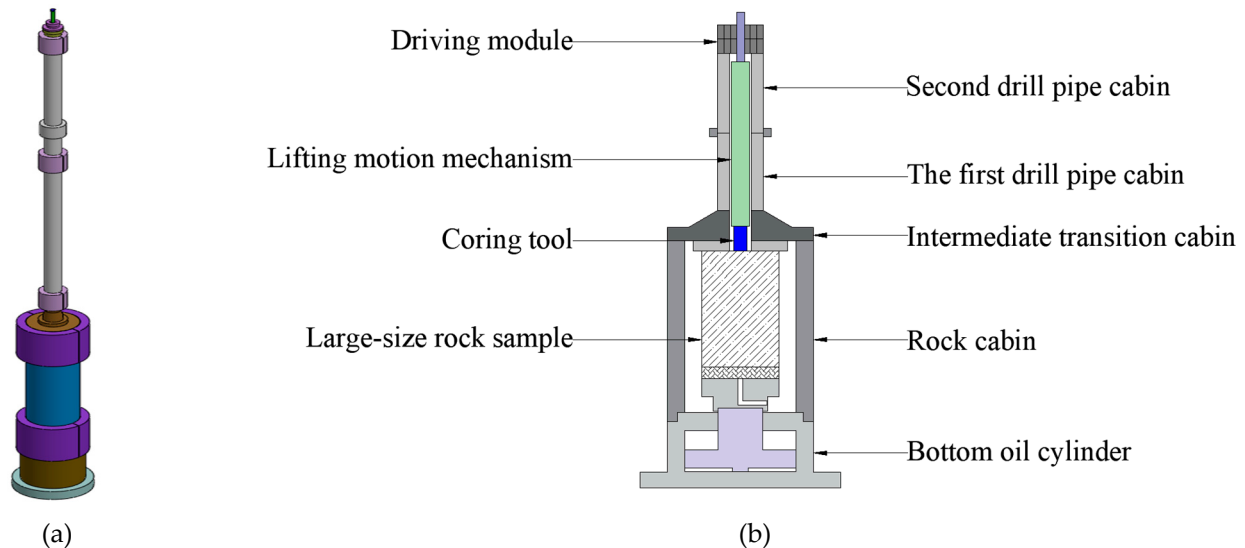


Figure 4. Overall structure of the simulation test cabin. (a) 3D model. (b) Two-dimensional cross-section.

3.1.2. The Structural Form of the Cabin

The maximum working pressure of the simulation test chamber designed in this paper is 140 MPa, and the maximum working temperature is 150 °C. Therefore, there are many design differences between this simulation test cabin and a cylinder under normal temperature and pressure, including the structural form, material, and wall thickness. At present, many research institutions have adopted various cylindrical structures for simulation test devices. The most commonly used structures are single-layer integral forged thick-walled cylinders, integral forged self-reinforcing thick-walled cylinders, double-layer and multilayer thick-walled cylinders, wire-wound cylinders, split block cylinders, and interlayer charging cylinders [30]. The bearing capacities for cylinders with different structural forms are not the same; the bearing capacity of a double-layer or multilayer cylinder is higher than that of a single-layer cylinder, and self-reinforced or prestressed structures carry higher loads than structures that are not self-reinforced or prestressed. Each cylinder structure has corresponding advantages and limiting factors. Therefore, in designing the structural form of the cylinder, all factors should be fully considered to choose a correct and reasonable structural form that meets usage requirements and is economical.

Figure 5 [39] shows the relationships between the ratio of the outer diameter to the inner diameter of cylinders with various structural forms and the pressures they bear. Based on Figure 5, the simulation test chamber in this paper was designed with a single-layer cylindrical structure to meet the usage requirements. The ranges and characteristics of various cylinder forms are listed in Table 1 [39]. Based on a comparison of various types of cylinder structures and economic considerations for manufacturing, a single-layer integral forged thick-walled cylinder was chosen for the test cabin.

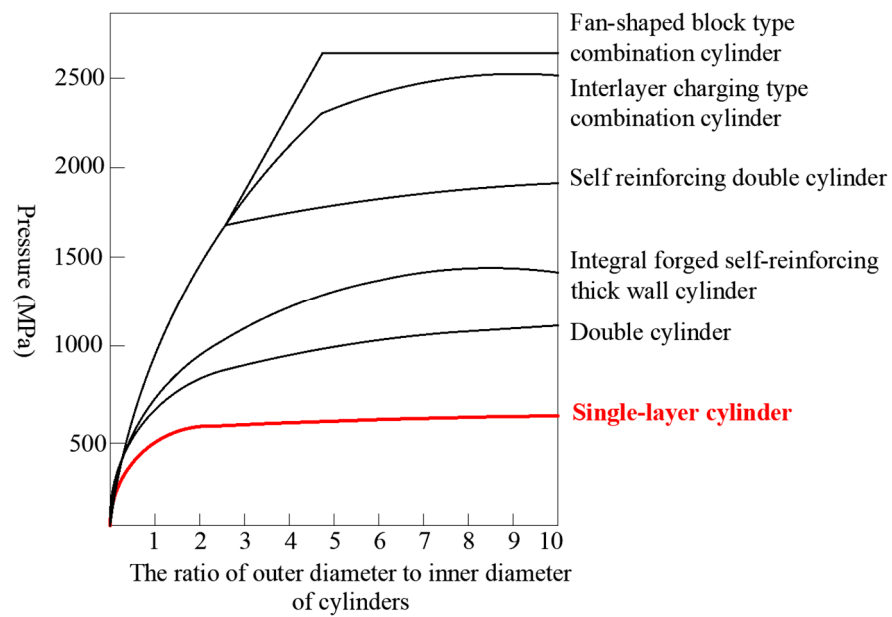


Figure 5. Bearing capacities of various cylindrical structures.

Table 1. Structural characteristics and application range for each cylinder form.

Structural Style	Characteristic	Scope of Application
Single-layer cylinder	Integral forging	Due to the limitation of forging conditions and high cost, it is suitable for steel with poor welding performance
	Roll-welded cylinder	Simple process, short cycle, high efficiency; however, it cannot be used when the cylinder diameter is too small
	Segmentally welded cylinder	Does not need large coil equipment; low productivity
	Seamless tubular cylinder	The source of raw materials is convenient, the manufacturing efficiency is high, and the cycle is short
		The diameter of the cylinder is between 300 mm and 800 mm, and the length does not exceed 12 m
		The diameter of the cylinder is greater than 400 mm, and the maximum thickness is 110 mm
		The larger the diameter is, the longer the manufacturing time
		The diameter of the cylinder should not exceed 500 mm

3.1.3. Analysis and Calculation of Wall Thickness

(1) Material selection

The materials used in the design and manufacture of the simulation test cabin must be provided by the manufacturer with the required material parameters. Key parameters for materials used in ultrahigh-pressure vessels have been stipulated in the literature [40] and are shown in Table 2.

Table 2. Material property specifications for ultrahigh-pressure vessels.

Percent Elongation after Fracture	Charpy Impact Work	Fracture Toughness	Area Reduction
≥16%	≥41 J	≥120 MPa	≥40%

According to the requirements for materials used in the simulation test cabin and the need for economy, the material chosen for the test chamber designed in this paper was 35CrNi3MoVR. The mechanical properties of the material at room temperature are shown in Table 3, and the mechanical properties at 150 °C are shown in Table 4 [40].

Table 3. Mechanical properties of 35CrNi3MoVR at room temperature.

Yield Strength, MPa	Strength of Extension, MPa	Percent Elongation after Fracture	Area Reduction	Shock Absorption Energy	Lateral Expansion, mm
≥960	1070–1230	≥16	≥45	≥47	≥0.53

Table 4. Mechanical properties of 35CrNi3MoVR at 150 °C.

Mark	Intensity Index	Date
35CrNi3MoVR	Yield strength	≥857 MPa
	Strength of extension	≥1060 MPa

According to the performance parameters given for 35CrNi3MoVR in Tables 3 and 4, the wall thickness of the rock cabin and drill pipe cabin were designed to provide a room temperature yield strength of $R_{p0.2} = 960$ MPa and a tensile strength of $R_m = 1070$ MPa. At a design temperature of 150 °C, the yield strength and tensile strength were

$R_{p0.2}^t = 857$ MPa and $R_m^t = 1060$ MPa, respectively. In this paper, the tensile test data for materials were used to calculate the thickness of the cylinder. The strength reduction coefficient of materials at 150°C was calculated as shown in Equation (1), which is 0.9.

$$\phi = 1 - \frac{T - 50}{1000} \quad (1)$$

where ϕ is the strength reduction coefficient of materials, and T is the temperature.

(2) Calculation of wall thickness

The failure criteria for pressure vessels mainly include elastic failure, plastic failure, and blasting failure criteria. The elastic failure criterion has been widely used and is poorly understood. Container elastic failure indicates that when the cylinder is subjected to internal pressure or other complex working loads, the stress on the cylinder wall is higher than the yield strength, and the container cannot continue to work normally. Plastic failure refers to the condition that, even though the local stress of the cylinder has exceeded the yield strength of the material and the material has undergone plastic deformation, as long as the cylinder material has not entered the full yield state, the container is not considered to have failed. Only when the whole container wall has completely undergone plastic deformation will the container fail [41,42].

The material properties of a single-layer integral forged thick-walled cylinder include high strength and good plasticity. When all materials in the cylinder yield, the increase in plastic deformation of the material leads to strain hardening and wall thinning. When the effect of strain hardening is stronger than the effect of wall thinning, the bearing capacity of the cylinder is enhanced. When the two effects are equivalent, the bearing capacity of the cylinder reaches the limit. If the load is increased further, the influence of wall thinning is more significant, which results in a decreased bearing capacity of the cylinder. When a certain pressure is reached, the container bursts, and blasting failure occurs. The materials used in ultrahigh-pressure vessels are generally high-strength materials rather than ideal plastic materials; with increases in the internal pressure of the container, the material gradually yields and then enters the plastic deformation phase. Due to material strain hardening, the container carrying capacity increases until blasting, and the bearing pressure at this time is called the burst pressure. The blasting failure process for container materials is illustrated in Figure 6 [39].

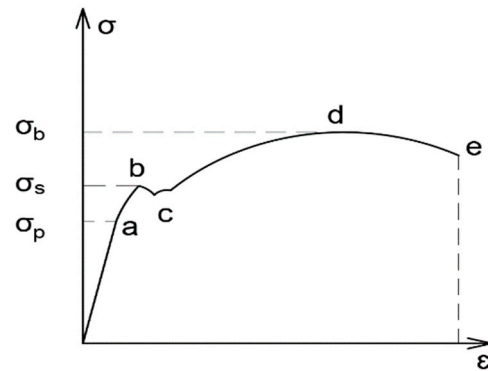


Figure 6. Failure process for nonideal plastic materials.

Although there are many methods for calculating the blasting failure criterion for a thick-walled pressure vessel, the Faupel formula is most widely used in practical engineering, and its derivation proceeds is as follows [43–46]:

The yield pressure of the vessel in the full yield state is:

$$p_s = \frac{2}{\sqrt{3}} R_{p0.2} \ln(K) \tag{2}$$

where p_s is the full yield pressure, MPa; $R_{p0.2}$ is the yield strength of the material at room temperature, MPa; and K is the ratio of the outside diameter to the inside diameter of the container.

Therefore, the bursting pressure can be written as:

$$p_b = \frac{2}{\sqrt{3}} R_m \ln(K) \tag{3}$$

where p_b is the blasting pressure, MPa and R_m is the tensile strength of the material at room temperature, MPa.

The formula for the calculation of burst pressure can be modified as follows:

$$p_b = \frac{R_{p0.2}}{R_m} \left(\frac{2}{\sqrt{3}} R_m \ln(K) \right) + \left(1 - \frac{R_{p0.2}}{R_m} \right) \left(\frac{2}{\sqrt{3}} R_{p0.2} \ln(K) \right) \tag{4}$$

The final burst pressure is:

$$p_b = \left(2 - \frac{R_{p0.2}}{R_m} \right) \frac{2}{\sqrt{3}} R_{p0.2} \ln(K) \tag{5}$$

The wall thickness of the simulation test cabin designed in this paper was calculated with the Faupel formula (Equation (5)). Because the simulation test chamber operates in a high-temperature and ultrahigh-pressure environment, all cylinders are subjected to high temperature and high pressure at the same time. Therefore, when calculating the thickness of the test chamber wall, the thermal load should be converted into a certain pressure and included in the design pressure, which can be converted as shown in Equation (6).

$$P_D = \phi \left(\frac{p_b}{n_b} \right) \tag{6}$$

In this formula, P_D is the design pressure; because the design pressure of the cabin body should not be lower than its maximum working pressure, 1.08 times the working pressure should be used as the design pressure. ϕ is the strength reduction coefficient of the material at the design temperature, which is calculated to be 0.9 according to Equation (1). n_b is the blasting safety factor of the cabin, which should be greater than or equal to 2.2 when calculated from tensile test data. Considering the economy of equipment

manufacturing and the safety of use, the blasting safety factor of the rock cabin designed in this paper is 2.5. As the total length of drill pipe cabin is 5 m, to avoid the instability of equipment caused by large axial deformation during operation, its blasting safety factor is further increased to 3. Therefore, the wall thickness calculation formula can be derived as follows [39].

$$\ln(K) = \frac{P_b}{\frac{2}{\sqrt{3}}R_{P0.2}(2 - \frac{R_{P0.2}}{R_m})} = \ln(\frac{R_i + \delta}{R_i}) \quad (7)$$

where R_i is the inner radius, mm and δ is the wall thickness, mm.

Therefore,

$$\delta = \frac{D_i}{2} \left[\exp\left(\frac{\sqrt{3}n_b P(D)}{2\phi R_{P0.2}(2 - \frac{R_{P0.2}}{R_m})}\right) - 1 \right] \quad (8)$$

where D_i is the inner diameter, mm.

The wall thickness required for a rock cabin with an inner diameter of 500 mm was calculated with Equation (8) as follows:

$$\delta = \frac{D_i}{2} \left[\exp\left(\frac{\sqrt{3}n_b P(D)}{2\phi R_{P0.2}(2 - \frac{R_{P0.2}}{R_m})}\right) - 1 \right] = \frac{500}{2} \left[\exp\left(\frac{\sqrt{3} \times 2.5 \times 140 \times 1.08}{2 \times 0.9 \times 960 \times (2 - \frac{960}{1070})}\right) - 1 \right] = 102.49 \text{ mm}$$

The wall thickness required for a drill pipe cabin with an inner diameter of 150 mm was calculated as follows:

$$\delta = \frac{D_i}{2} \left[\exp\left(\frac{\sqrt{3}n_b P(D)}{2\phi R_{P0.2}(2 - \frac{R_{P0.2}}{R_m})}\right) - 1 \right] = \frac{150}{2} \left[\exp\left(\frac{\sqrt{3} \times 3 \times 140 \times 1.08}{2 \times 0.9 \times 960 \times (2 - \frac{960}{1070})}\right) - 1 \right] = 38.27 \text{ mm}$$

Therefore, when 1.08 times the maximum working pressure was taken as the design pressure and blasting failure was adopted as the design criterion, the wall thickness of the rock cabin was 102.49 mm and that of the drill pipe cabin was 38.27 mm. In actual working conditions, the influence of added thickness and manufacturing deviations should be considered, so the thickness of rock cabin should be increased to 107.5 mm and that of drill cabin was rounded up to 40 mm.

Therefore, the inner diameter of the rock cabin is 500 mm and that the outer diameter is 715 mm. The inside diameter of the drill pipe cabin is 150 mm, and the outside diameter is 230 mm. In the calculations of wall thickness for each section of the cabin, the thermal load and pressure on the test cabin were considered simultaneously. Theoretically, the calculated wall thickness can bear an ultrahigh pressure of 140 MPa and a temperature of 150 °C at the same time.

3.2. Driving Module for Simulating Coring Tests

The driving module consists of two parts: a dynamic system and a lifting motion mechanism. The dynamic system provides weight on bit, torque and speed for simulated coring tests and provides a dynamic sealing function for the upper part of the device. The lifting motion mechanism is used to connect the power system to the pressure-preserving coring tool, to transfer weight on bit and torque, and to assist in the function of the coring tool.

3.2.1. Structure and Working Principle of the Lifting Motion Mechanism

In an actual field coring process, rotational and vertical downward coring movements must be completed. To maintain the core pressure after the core enters the core barrel, it must be pulled into the core device, which provides similar environmental conditions. Because the rotary drive pump station can provide only rotary coring motion, it cannot provide the downward feeding motion. Therefore, the lifting mechanism in the cabin was designed independently to realize the vertical downward coring motion and core lifting motion after drilling. The lifting mechanism in the cabin was mainly composed of a

rotating shaft, rotating piston, core lifting mechanism, rotating piston joint, and corer joint, as shown in Figure 7.

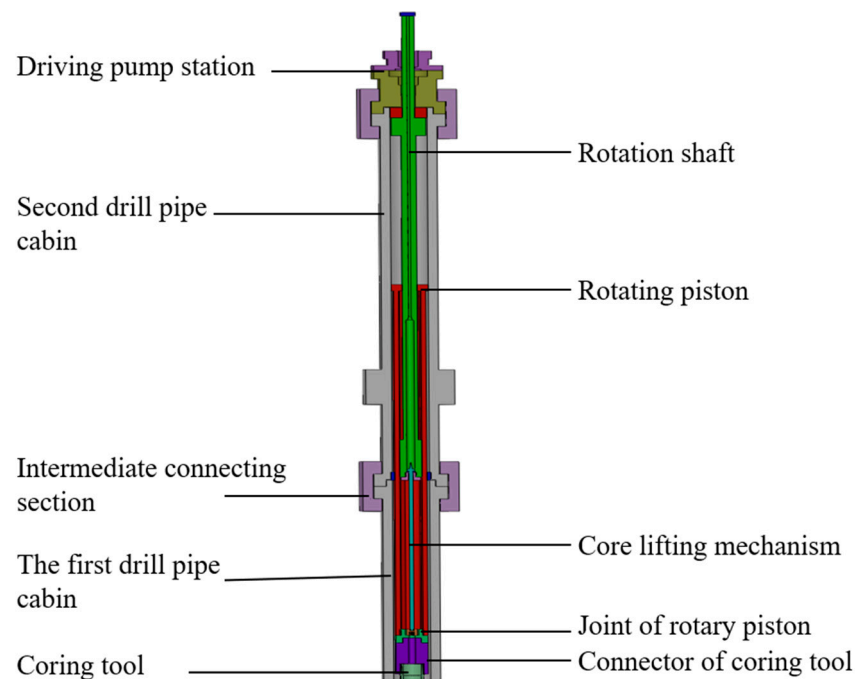


Figure 7. Structure of the lifting motion mechanism.

The working principle of the lifting motion mechanism is as follows: The rotation shaft is driven by the rotating pump station, and a spline connection is placed between the rotating piston and the rotating drive shaft, so the rotating shaft causes the piston to rotate. Additionally, the rotary piston is driven by the drilling pressure and moves downward in a straight line. Furthermore, power is transferred to the upper part of the corer by rotating the piston joint and the upper part of the corer, thus initiating the coring motion. After the coring motion is completed, the drilling pressure is reduced, and the piston is moved upward by the pressure difference; the corer joint and coring device form a threaded connection, and the rotating piston joint and coring device jointly adopt the form of a spline connection to release the spline. This part of the rotating piston connection moves upward, driving up the core-lifting mechanism to complete the coring motion.

3.2.2. Composition of the Dynamic System

This system includes the driving pump station and an ultrahigh-pressure rotary dynamic sealing system [6], and the main function is to provide a power source for simulated coring tests and activation of the pressure seal inside the cabin. The ultrahigh-pressure rotary sealing structure consists of three groups of sealing rings, as shown in Figure 8. Each set of sealing rings comprise an “O”-type rubber ring, a “Z”-type sealing ring with grooves on the inner surface, and a supporting sleeve. Among them, the “Z” ring is made of polytetrafluoroethylene (PTFE). PTFE has the advantages of a low friction coefficient and high wear resistance, and it can adapt to ultrahigh-pressure rotary dynamic sealing conditions. On this basis, a pair of combined grooves is provided on the main sealing surface and matched with the rotating axis of the “Z” ring. Combined grooves can cover impurities and prevent the sealing surface from being damaged. Additionally, lubricating oil can be stored inside the combined grooves and produce a lubricating oil film on the main sealing surface during operation and effectively prevent wear and destruction of the main sealing surface.

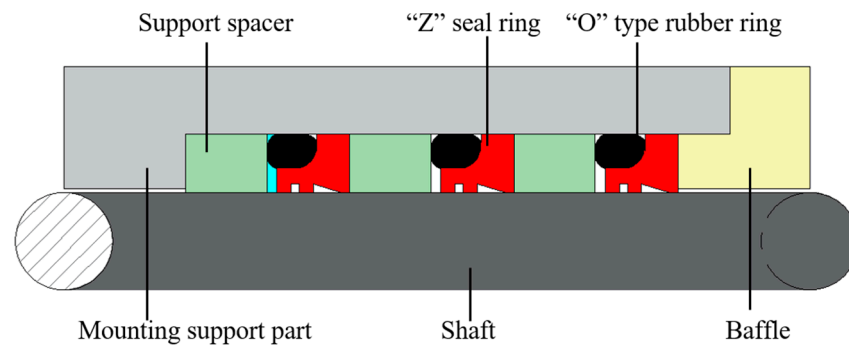


Figure 8. Ultrahigh-pressure rotary dynamic sealing structure.

4. Experimental Study and Results Analysis of the Device

The in-situ simulation device for testing deep coring tools is composed of two main modules. The high-temperature and ultrahigh-pressure simulation test cabin needs to operate under the ultrahigh-pressure of 140 MPa and the high-temperature of 150 °C, so the influence of temperature and pressure on the deformation of the cabin was taken into account during the experiment. However, the driving module is located at the upper end of the drill pipe cabin and far away from the rock cabin. Meanwhile, in Section 3.2.1 of this paper, the rotating piston set in the lifting motion mechanism can play a role in isolating the high-temperature fluid in the rock cabin. Therefore, the driving module mainly works under the ultrahigh-pressure of 140 MPa, and the influence of temperature on it can be ignored. In this section, experimental studies are carried out on the two modules of the device respectively. The results show that the design of the device is reasonable, and the stability of the working performance of the device in deep extreme environment is verified.

4.1. Pressure Testing and Results Analysis of the Test Cabin

In this study, a hydraulic pressure test was carried out with the rock cabin and drill pipe cabin, and the pressure pump of a Sichuan jet was used for pressure testing, as shown in Figure 9. Considering the influence of temperature and pressure on the cabin body, the minimum test pressure, P_t , was calculated with Equation (9) [40] below, and the minimum test pressure at room temperature was 189.70 MPa. Therefore, a test pressure of 190 MPa meets the use requirements.

$$P_t = 1.12P_D \frac{R_{P0.2}}{R_{P0.2}^t} = 1.12 \times 140 \times 1.08 \times \frac{960}{857} = 189.70 \text{ MPa} \quad (9)$$



Figure 9. Pressure pump produced for a Sichuan jet.

4.1.1. Pressure Testing of the Rock Cabin

The inner diameter of the rock cabin was 500 mm, and the length was 2400 mm. During the experiment, hydraulic oil is injected into the interior of the cabin body through pressure testing pump to achieve pressure application, and the axial deformation of the rock cabin was detected. Due to the symmetrical structure of the rock cabin, deformation data for only one end face should be recorded when axial deformation is detected, and it should then be multiplied by 2 to obtain the total axial deformation. Therefore, in pressure tests of the rock cabin, an axial displacement detection meter was placed on the end face to measure axial deformation, as shown in Figure 10. The original reading of the displacement detector during the test and the data after modification are provided in Table 5.



Figure 10. Pressure system for testing the rock cabin.

Table 5. Axial deformation of the rock cabin.

Test Pressure, MPa	Axial Displacement Test Data, mm	Unilateral Axial Deformation, mm	Total Axial Deformation, mm
0	1.000	0	0
50	1.865	0.865	1.730
100	2.769	1.769	3.538
150	3.742	2.742	5.484
190	4.490	3.490	6.980

As shown in Table 5, the second column is the original reading of the axial displacement detector during the test. Because the initial reading of the axial displacement detector is 1 mm when the pressure is 0 MPa, the data recorded by the displacement detector should be subtracted from the initial readings to obtain the real axial displacement of one side, as shown in the second column of Table 5. Meanwhile, the axial displacement of one side should be multiplied by 2 to obtain the total axial deformation of the cabin, as shown in the third column of Table 5. The relation curves between the axial displacement and test pressure are shown in Figure 11.

According to Figure 11, with the gradual increase of the test pressure, the axial deformation of the rock cabin also increases gradually and presents a linear growth trend with the change of the pressure. When the highest pressure is 190 MPa, the total axial deformation reaches the maximum value of 6.980 mm, and the relative deformation is 0.291%. Therefore, in the process of the internal pressure of the rock cabin rising from 0 MPa to 190 MPa, the axial deformation of the cabin body is always in the stage of elastic deformation, and the deformation is small. At the same time, no leakage of pressure or flow was detected on the outer surface of the cabin during the test. Therefore, the design of the cabin is reasonable.

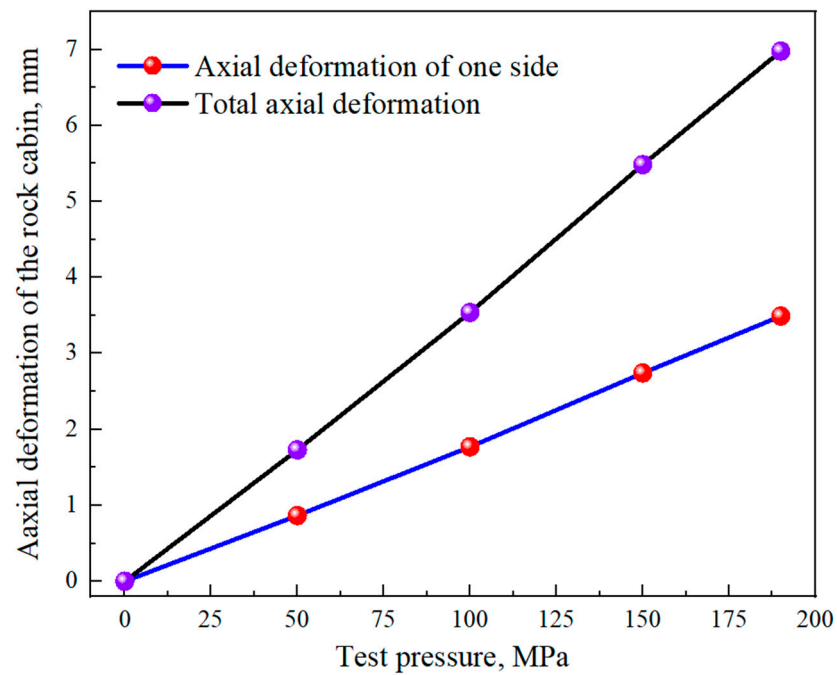


Figure 11. Axial deformation of the rock cabin.

4.1.2. Pressure Testing of the Drill Pipe Cabin

The drill pipe cabin had an inner diameter of 150 mm, an outer diameter of 230 mm, and a total length of 5000 mm. Because the inner diameter of the cabin was small, primarily axial displacement occurred during use. However, the design of the wall thickness was sufficient. Therefore, the main purpose of the pressure test on the drill pipe cabin was to detect axial deformation. Due to the asymmetrical structure of the two drill pipe cabins, axial displacement detector 1 should be placed on the lower end face of the first drill pipe cabin, and axial displacement detector 2 should be placed on the upper end face of the second drill pipe cabin to record the axial displacement of the drill pipe cabin during testing, as shown in Figure 12. In addition, the total axial deformation for each drill pipe cabin should be the sum of two deformations. The axial deformation data after processing are shown in Table 6. The plots of axial deformation vs. test pressure are shown in Figure 13.



Figure 12. Drill pipe cabin test system.

Table 6. Data for axial deformation of the drill pipe cabin.

Test Pressure, MPa	Axial Displacement 2, mm	Axial Displacement 1, mm	Total Axial Deformation, mm
0	0	0	0
50	0.285	0.350	0.635
100	0.567	0.630	1.197
150	0.873	0.932	1.805
190	1.115	1.194	2.309

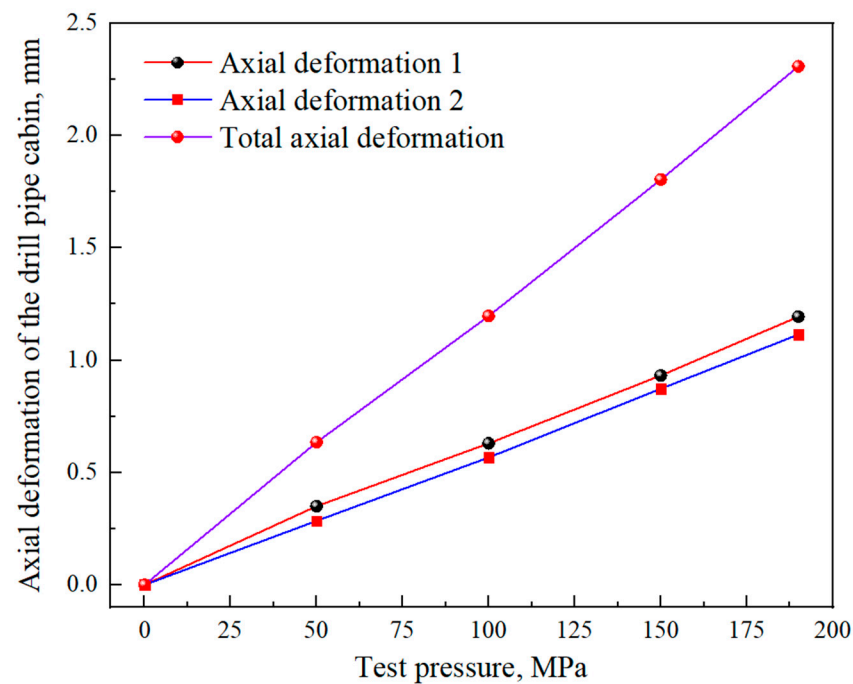


Figure 13. Axial deformation of the drill pipe cabin.

According to Figure 13, when the internal pressure of the drill pipe chamber rises, the axial deformation detected at both ends of the drill pipe cabin presents a linear increase trend with the increase of pressure, indicating that the drill pipe cabin was always in the elastic deformation stage under the pressure condition of 0 MPa to 190 MPa, and can operate safely and stably. Furthermore, it is found that the deformation data of the two detectors are close to each other, which indicates that the deformation of one end is half of the total axial deformation of the drill pipe cabin, as long as their structure is consistent, even if the length of the two drill pipe cabins is not consistent. Meanwhile, under the condition of maximum pressure of 190 MPa, the maximum deformation of the drill pipe cabin is 2.309 mm, and the relative deformation is 0.046%, which is greatly reduced compared with that of rock sample chamber, which is 0.291%. It is further explained that, in the calculation of the wall thickness of the drill pipe cabin in Section 3.1.3 of this paper, considering that the drill pipe cabins are slender tubes, it is reasonable to adjust the safety factor upward to 3 to ensure its small deformation under ultrahigh-pressure. Therefore, the drill pipe cabin can operate stably in the extreme environment of ultrahigh-pressure. Its structure selection is reasonable, and the calculation of wall thickness is reliable.

4.2. Experimental Study of the Driving Module

4.2.1. The Composition and Working Principle of the Experimental System

Because the high temperature load of 150 °C is mainly applied to the rock cabin, the driving module only works under the ultrahigh-pressure condition of 140 MPa, without the influence of high temperature. To verify the performance of the driving module, ultrahigh-pressure dynamic system experimental equipment was independently developed; it mainly comprised a driving pump station, an ultrahigh-pressure cabin, a rotating shaft, and an ultrahigh-pressure hydraulic station, as shown in Figure 14. At the same time, the ultrahigh pressure rotary dynamic sealing structure is installed between the inner surface of the ultrahigh pressure cabin and the rotating shaft (the diameter is 50 mm). The ultrahigh-pressure hydraulic station can provide a pressure of 140 MPa for high-pressure conditions. In the lifting motion mechanism in Section 3.2.1, a rotating piston is adopted to isolate the high-temperature fluid at the lower part, and normal temperature fluid is passed into the upper space of the rotary piston to complete the application of bit weight. Therefore,

the driving module only works in the high-pressure environment of 140 °C, without considering the influence of temperature.

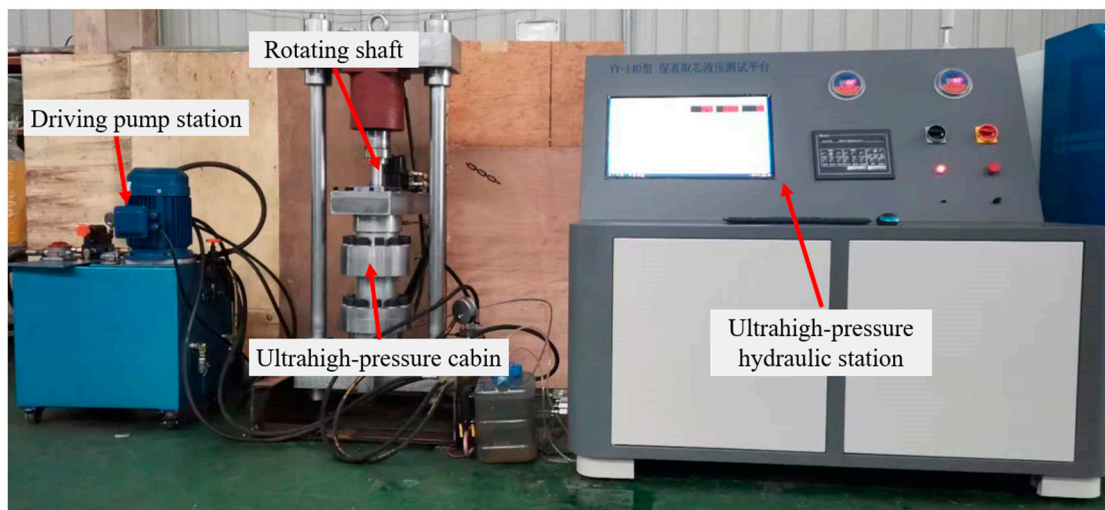


Figure 14. Ultrahigh-pressure dynamic system experimental equipment.

The performance of the driving module is studied experimentally with this system. The high-pressure fluid is injected into the ultrahigh-pressure cabin through the ultrahigh-pressure hydraulic station to achieve the pressure required by the experiment. Meanwhile, the driving pump station is used to provide power for the rotating shaft to complete the application of rotation speed.

4.2.2. Results and Analysis

In order to facilitate analysis, the test data were plotted as curves, as shown in Figures 15–17. Figure 15 shows the curve of test pressure changing with time, Figure 16 shows the curve of rotation speed changing with time, and Figure 17 shows the curve of rotation speed and test pressure.

As shown in Figures 15 and 16, both pressure and rotation speed are applied in two steps. In the first stage, the pressure is increased to 10 MPa and the rotation speed is increased to 60 r/min within 1 min, and the working condition is maintained for approximately 3 min. By observing the curve of test results, it is found that the pressure remains stable, and the rotation speed of the rotating shaft is basically unchanged. Therefore, under the condition of low pressure and low rotation speed, the test system can run normally, which preliminarily verifies the stability of the test system function.

On this basis, the pressure is further increased from 10 MPa to 140 MPa and the rotation speed from 60 r/min to 150 r/min within 1 min, and the stable running time is 105 min under this condition. There is no leakage of flow or pressure in the whole test process. Therefore, under the extreme conditions of ultrahigh-pressure of 140 MPa and rotation speed of 150 r/min, the driving pump station can provide a stable power source, and the sealing structure has good sealing performance.

Furthermore, the rotation speed was reduced from 150 r/min to 142 r/min and maintained for 15 min under the condition that the ultrahigh-pressure was maintained at 140 MPa. The test system can also run stably. The rotation speed was further reduced, as shown in Figure 17. No leakage of pressure or flow was detected during the test. Therefore, the driving module can operate safely and stably without pressure or flow leakage risk by reducing rotation speed under the condition of maintaining constant ultrahigh-pressure. It is suggested that the rotating speed should be reduced first and then the pressure should be reduced after the test with the in-situ deep simulation coring device.

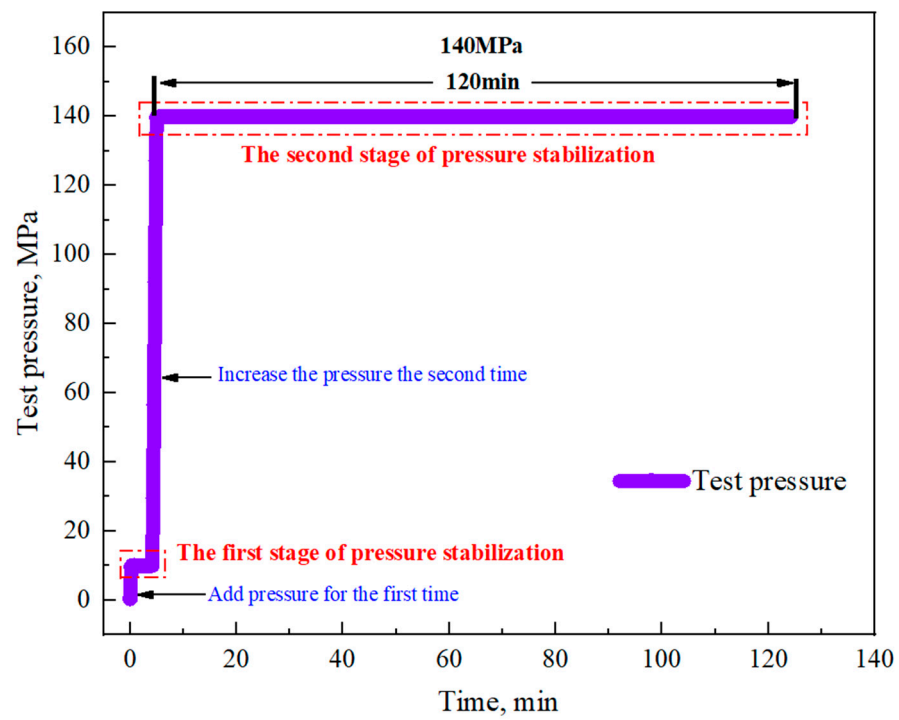


Figure 15. Test pressure vs. time.

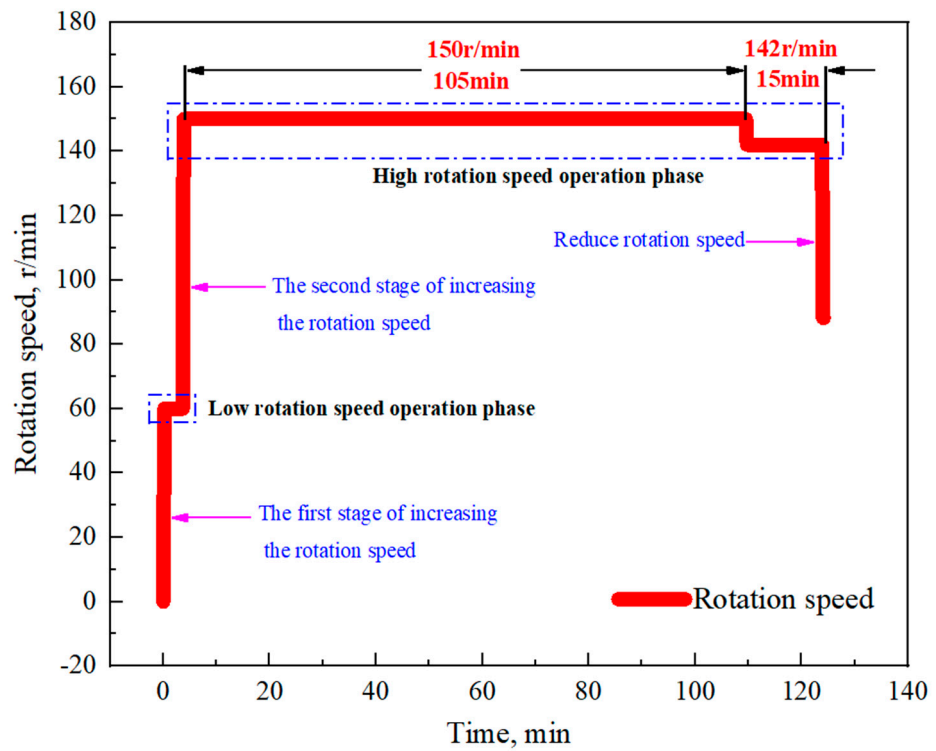


Figure 16. Rotation speed vs. time.

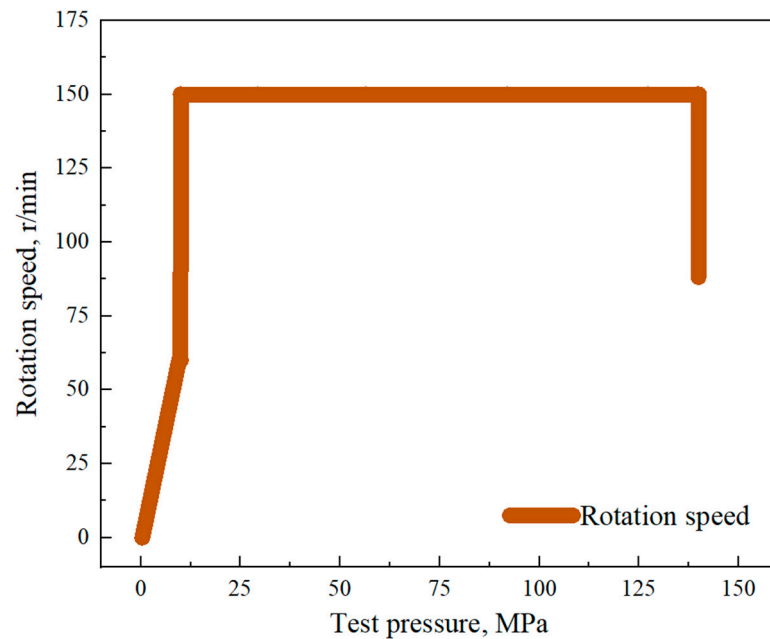


Figure 17. Rotation speed vs. test pressure.

5. Conclusions

In this study, an in-situ simulation device for testing deep pressure-preserving coring tools under high-temperature and ultrahigh-pressure was developed, and the simulation principle and method for this extreme environment were expounded. Furthermore, the high-temperature and ultrahigh-pressure simulation test cabin and the driving module of the device were analyzed and experimentally studied. The main conclusions are as follows:

(1) In this study, a simulated coring test system with a working pressure of 140 MPa and a temperature of 150 °C was established. On the basis of analyzing the stress state of rock in deep extreme environments, the principle and method of constructing the temperature and pressure conditions of the test cabin are proposed.

(2) Based on the design standard of ultrahigh-pressure vessels, a segmented high-temperature and ultrahigh-pressure coring simulation test cabin was innovatively constructed. A pressure test was conducted on the cabin body by setting different pressure values. The results showed that the test cabin operated stably under the maximum pressure of 190 MPa (the effect of temperature of 150 °C has been translated into pressure for experiments), and there was no pressure or fluid leakage during the test. The test cabin exhibited good performance. Therefore, the design and manufacture of the cabin have high reliability, which has important reference value for the development of ultrahigh-pressure vessels for extreme environments.

(3) The experimental study of the driving module showed that this module could run stably for 105 min under the conditions that the axis diameter is 50 mm, the test pressure is 140 MPa, and the rotation speed is 150 r/min (the highest tested), which provides a stable power source for the coring simulation. When the pressure is maintained at 140 MPa, the driving module can operate safely and stably by reducing the rotation speed of the rotating shaft. Therefore, after the completion of the test with the in-situ simulation device, the safe operation mode of reducing the speed first and then depressurizing the pressure can be adopted.

(4) The in-situ simulation device innovatively developed in this study can realize the simulation of the in-situ extreme environment of deep rock occurrence. Further, it can be used for the research and development of deep pressure-preserving coring tools, which effectively avoids the problems of high risk and high cost in field testing of coring tools.

Author Contributions: Conceptualization, W.H. and Z.Z.; data curation, Y.Y. and Y.L.; methodology, W.H. and Z.H.; supervision, H.X.; writing—original draft preparation, W.H.; writing—review and editing, J.L. and C.L. All authors have read and agreed to the published version of the manuscript.

Funding: This research was funded by the Program for Guangdong Introducing Innovative and Entrepreneurial Teams (Grant No. 2019ZT08G315) and the National Natural Science Foundation of China (Grant No. 51827901, U2013603).

Institutional Review Board Statement: Not applicable.

Informed Consent Statement: Informed consent was obtained from all subjects involved in the study.

Data Availability Statement: The data presented in this study are available on request from the corresponding author.

Acknowledgments: The authors would like to thank the editors and reviewers for their valuable comments and constructive suggestions.

Conflicts of Interest: The authors declare that there is no conflict of interest.

References

- Xie, H.P.; Konietzky, H.; Zhou, H.W. Special Issue “Deep Mining”. *Rock Mech. Rock Eng.* **2019**, *52*, 1415–1416. [\[CrossRef\]](#)
- Xie, H.P.; Gao, F.; Ju, Y. Research and development of rock mechanics in deep grand engineering. *Chin. J. Rock Mech. Eng.* **2015**, *34*, 2161–2178. [\[CrossRef\]](#)
- Yang, J.P.; Chen, L.; Gu, X.B.; Zhao, Z.Y.; Fu, C.H.; Yang, D.S.; Tian, D.Z.; Chen, Z.S.; Xie, H.P. Hollow glass microspheres/silicone rubber composite materials toward materials for high performance deep in-situ temperature-preserved coring. *Pet. Sci.* **2022**, *19*, 309–320. [\[CrossRef\]](#)
- He, Z.Q.; Yang, Y.; Yu, B.; Yang, J.P.; Jiang, X.B.; Tian, B.; Wang, M.; Li, X.Y.; Sun, S.Q.; Sun, H. Research on properties of hollow glass microspheres/epoxy resin composites applied in deep rock in-situ temperature-preserved coring. *Pet. Sci.* **2022**, *19*, 720–730. [\[CrossRef\]](#)
- Zhang, Q.G.; Fan, X.Y.; Chen, P.; Ma, T.S.; Zeng, F.T. Geomechanical behaviors of shale after water absorption considering the combined effect of anisotropy and hydration. *Eng. Geol.* **2020**, *269*, 105547. [\[CrossRef\]](#)
- Huang, W.; Feng, G.; He, H.L.; Chen, J.Z.; Wang, J.Q.; Zhao, Z. Development of an ultra-high pressure rotary combined dynamic seal and experimental study on its sealing performance in deep energy mining conditions. *Pet. Sci.* **2022**, *19*, 1305–1321. [\[CrossRef\]](#)
- Xie, H.P. Research framework and anticipated results of deep rock mechanics and mining theory. *Adv. Eng. Sci.* **2017**, *49*, 1–16. [\[CrossRef\]](#)
- Li, C.; Pei, J.L.; Wu, N.H.; Liu, G.K.; Huang, W.; Dai, Z.X.; Wang, R.Z.; Chen, Z.F.; Long, W.C. Rotational failure analysis of spherical-cylindrical shell pressure controllers related to gas hydrate drilling investigations. *Pet. Sci.* **2022**, *19*, 789–799. [\[CrossRef\]](#)
- Gao, M.Z.; Yang, B.G.; Xie, J.; Ye, S.Q.; Liu, J.J.; Liu, Y.T.; Tang, R.F.; Hao, H.C.; Wang, X.; Wen, X.Y.; et al. The mechanism of microwave rock breaking and its potential application to rock-breaking technology in drilling. *Pet. Sci.* **2022**, *19*, 1110–1124. [\[CrossRef\]](#)
- Wang, G.; Qin, X.J.; Han, D.Y.; Liu, Z.Y. Study on seepage and deformation characteristics of coal microstructure by 3D reconstruction of CT images at high temperatures. *Int. J. Min. Sci. Technol.* **2021**, *31*, 175–185. [\[CrossRef\]](#)
- Xie, H.P.; Liu, T.; Gao, M.Z.; Chen, L.; Zhou, H.W.; Ju, Y.; Gao, F.; Peng, X.B.; Li, X.J.; Peng, R.D.; et al. Research on in-situ condition preserved coring and testing systems. *Pet. Sci.* **2021**, *18*, 1840–1859. [\[CrossRef\]](#)
- Gao, M.Z.; Hao, H.C.; Xue, S.N.; Lu, T.; Cui, P.F.; Gao, Y.N.; Xie, J.; Yang, B.G.; Xie, H.P. Discing behavior and mechanism of cores extracted from Songke-2 hole at depths below 4500 m. *Int. J. Rock Mech. Min. Sci.* **2022**, *149*, 104976. [\[CrossRef\]](#)
- Gao, M.Z.; Xie, J.; Gao, Y.N.; Wang, W.Y.; Li, C.; Yang, B.G.; Liu, J.J.; Xie, H.P. Mechanical behavior of coal under different mining rates: A case study from laboratory experiments to field testing. *Int. J. Min. Sci. Technol.* **2021**, *31*, 825–841. [\[CrossRef\]](#)
- Zhang, Q.G.; Wang, Z.X.; Fan, X.Y.; Wei, N.; Zhao, J.; Lu, X.W.; Yao, B.W. A novel mathematical method for evaluating the wellbore deformation of a diagenetic natural gas hydrate reservoir considering the effect of natural gas hydrate decomposition. *Nat. Gas Ind. B* **2021**, *8*, 287–301. [\[CrossRef\]](#)
- Sun, Y.H.; Wang, Y.; Lü, X.S.; Jia, R.; Guo, W. Hole-bottom freezing method for gas hydrate sampling. *J. Nat. Gas Sci. Eng.* **2015**, *25*, 271–283. [\[CrossRef\]](#)
- Gao, M.Z.; Xie, J.; Guo, J.; Lu, Y.Q.; He, Z.Q.; Li, C. Fractal evolution and connectivity characteristics of mining-induced crack networks in coal masses at different depths. *Geomech. Geophys. Geo-Energy Geo-Resour.* **2021**, *7*, 9. [\[CrossRef\]](#)
- Hu, Y.Q.; Xie, J.; Xue, S.N.; Xu, M.; Fu, C.H.; He, H.L.; Liu, Z.Q.; Ma, S.M.; Sun, S.Q.; Wang, C.L. Research and application of thermal insulation effect of natural gas hydrate freezing corer based on the wireline-coring principle. *Pet. Sci.* **2022**, *19*, 1291–1304. [\[CrossRef\]](#)
- Li, J.N.; Wang, J.; Hu, Y.Q.; You, Z.X.; Xu, M.; Wang, Y.W.; Zou, Z.J.; Kang, Q.Y. Contact performance analysis of pressure controller’s sealing interface in deep in-situ pressure-preserved coring system. *Pet. Sci.* **2022**, *19*, 1334–1346. [\[CrossRef\]](#)

19. Zhu, L.Y.; Liu, T.; Zhao, Z.Y.; Wu, Y.F.; Yang, D.S.; Shi, X.C.; Liu, Z.Q.; Lu, F.F.; Qin, P.; Gao, X.L. Deep original information preservation by applying in-situ film formation technology during coring. *Pet. Sci.* **2022**, *19*, 1322–1333. [[CrossRef](#)]
20. Gao, M.Z.; Zhang, Z.L.; Yin, X.G.; Xu, C.; Liu, Q.; Chen, H.L. The location optimum and permeability-enhancing effect of a low-level shield rock roadway. *Rock Mech. Rock Eng.* **2018**, *51*, 2935–2948. [[CrossRef](#)]
21. Gao, M.Z.; Zhang, J.G.; Li, S.W.; Wang, M.; Wang, Y.W.; Cui, P.F. Calculating changes in the fractal dimension of surface cracks to quantify how the dynamic loading rate affects rock failure in deep mining. *J. Cent. South Univ. Technol.* **2020**, *27*, 3013–3024. [[CrossRef](#)]
22. Xu, J.J. Design of High Temperature High Pressure Simulation Test Device Program. Master's Thesis, China University of Geosciences, Beijing, China, 2021.
23. Zheng, J.H.; Zong, Y.B.; Qian, D.R.; Wang, L.; Wang, Q. Development of downhole environment simulation test equipment. *Sci. Technol. Eng.* **2017**, *17*, 21–25. [[CrossRef](#)]
24. Liu, X. Design and Research on High Pressure Simulated Shaft Heating System. Master's Thesis, Northeast Petroleum University, Daqing, China, 2018.
25. Luo, Q. Design and Experimental Research of Down-Hole Tools Simulation Test Bench. Master's Thesis, Yangtze University, Jinzhou, China, 2015.
26. Kong, R.; Luan, J.F.; Wang, C.L. Stress evaluation and reliability analysis for high temperature and high-pressure vessel in the discontinuous zone. *Ind. Heat.* **2016**, *45*, 30–32. [[CrossRef](#)]
27. Morandi, A.C.; Karunakaran, D.; Dixon, A.T.; Baerheim, M. Comparison of Full-Scale Measurements and Time-Domain Irregular Sea Analysis for a Large Deepwater Jack-Up. In Proceedings of the Offshore Technology Conference, Houston, TX, USA, 2–5 May 1998. [[CrossRef](#)]
28. Hooker, P.R.; Brigham, W.E. Temperature and heat transfer along buried liquids pipelines. *J. Pet. Technol.* **1978**, *30*, 747–749. [[CrossRef](#)]
29. Quigley, M.S.; Dzialowski, A.K.; Zamora, M. A Full-Scale Wellbore Friction Simulator. In Proceedings of the IADC/SPE Drilling Conference, Houston, TX, USA, 27 February–2 March 1990. [[CrossRef](#)]
30. Kabir, C.S.; Hasan, A.R.; Jordan, D.L.; Wang, X.W. A wellbore/reservoir simulator for testing gas holes in high-temperature reservoirs. *SPE Form. Eval.* **1996**, *11*, 128–134. [[CrossRef](#)]
31. Yang, L.Q. Study of the Full-Scale Drilling Simulating Test Device under the Condition of Bottom Hole Pressures. Master's Thesis, Zhejiang University, Hangzhou, China, 2002.
32. Xue, J. Overview of several foreign high temperature and high pressure simulation drilling test equipment. *Foreign Geexplor. Technol.* **1995**, *2*, 35–36.
33. Zhou, C.; Wang, X.D. Introduction of M150 simulated wellbore. *Drill. Eng.* **1993**, *3*, 16–17.
34. Zhang, F.M. Development of drilling tool test system in dagang oilfield. *Oil Field Equip.* **2009**, *384*, 72–78. [[CrossRef](#)]
35. Wei, L.S. Design of High Temperature and High Pressure Simulation Testing System for Instrument Development. Master's Thesis, Southwest Petroleum University, Chengdu, China, 2016.
36. Pang, D.X.; Wang, Z.M.; Pan, D. Development of high temperature and high pressure test equipment for downhole tools. *Hole Test.* **2017**, *26*, 45–48+51+77.
37. Xu, D.J.; Liu, H.; Wang, Y.; Zeng, L.X.; Wang, K.; Wang, X.J. The developing and using of downhole tools experimental facility under high temperature and high pressure condition. In *2018 the National Natural Gas Annual Symposium*; Natural Gas Professional Committee of Chinese Petroleum Society: Beijing, China, 2018. [[CrossRef](#)]
38. Zhang, W.H.; Zhang, H.T.; Wang, W.P. Development of high temperature and high pressure vertical hole simulation test device for downhole tools. *Mach. Des. Manuf. Eng.* **2020**, *49*, 31–34.
39. Ding, G.D. Design and Research on Simulation Test Shaft of High Temperature and High Pressure. Master's Thesis, China University of Petroleum, Beijing, China, 2014.
40. GB/T 34019-2017; Ultra-High Pressure Vessels. National Standards of People's Republic of China: Beijing, China, 2017.
41. Shao, G.H.; Wei, Z.C. *Ultra-High Pressure Vessel*; Chemical Industry Press: Beijing, China, 2002.
42. Wang, J.B. Safety Analysis and Accident Prevention of High Temperature and High Pressure Testing Equipment of Logging Tools. Master's Thesis, China University of Petroleum, Beijing, China, 2014.
43. Hu, X.M.; Wang, C.L.; Cai, X.L.; Li, Q.W.; Chen, B. Development of high-temperature and high-pressure reaction kettle system. *Mech. Eng. Autom.* **2013**, *3*, 153–155. [[CrossRef](#)]
44. Wang, Z.W.; Cai, R.L. *Pressure Vessel Design*; Chemical Industry Press: Beijing, China, 2005.
45. Liu, C.; Wu, S.L.; Yang, F.; Hong, K.; Zhang, S.; Liu, X.N. Precision comparison of calculation formulas for ultra-high pressure vessel burst pressure. *Press. Vessel Technol.* **2019**, *36*, 43–49+66. [[CrossRef](#)]
46. Chen, Z.W.; Li, T.; Yang, G.Y. Technical Progress in GB/T 34019—2017 Standard “Ultrahigh Pressure Vessel”. *Press. Vessel Technol.* **2019**, *36*, 46–51.

Disclaimer/Publisher's Note: The statements, opinions and data contained in all publications are solely those of the individual author(s) and contributor(s) and not of MDPI and/or the editor(s). MDPI and/or the editor(s) disclaim responsibility for any injury to people or property resulting from any ideas, methods, instructions or products referred to in the content.